Proceedings of the
International Conference on Mechanical Engineering 2003
(ICME2003) 26- 28 December 2003, Dhaka, Bangladesh

ICME03-FL-05

THREE DIMENSIONAL ANALYSIS AND APPLICATION OF A LINE SOLVER FOR THE RECIRCULATING FLOWS USING MULTIGRID METHODS.

T. M. Shah

Dr. A. Q. Khan Research Laboratories,
P. O. Box No. 502, Rawalpindi Pakistan

ABSTRACT

This paper is an extention of the earlier published work [?] Which was a 2D line solver for the Incompressible Navier-Stokes (NS) equations, carried out an analysis and application of a line solver for the recirculating flows using the multigrid methods. The work has been described a robust line solver for the coupled equations. The calculation procedure, called SCGS/LS (Symmetrical Coupled Gauss-Seidel/Line Solver), was based on the SCGS scheme. This technique is now applied to the 3d driven cavity problem for the recirculating flows. 3D Fourier analysis of the multigrid method is also carried out. The scheme is simple and easy to program as in the case of two dimensions. The rates of convergence and the computational times are reported for the test case.

Key words: NS equations, Multigrid methods, Line solver, Fourier Analysis, 3D driven Cavity problem

1. DIFFERENTIAL AND DIFFERENCE EQUATIONS

The equations expressing conservation of mass and momentum in three dimensions for an ideal, incompressible, Newtonian fluid are given by:

$$\frac{\partial \rho u}{\partial x}+\frac{\partial \rho v}{\partial y}+\frac{\partial \rho w}{\partial z}=0, \qquad (1)$$

$$\frac{\partial \rho u^2}{\partial x}+\frac{\partial \rho uv}{\partial y}+\frac{\partial \rho vw}{\partial z}=-\frac{\partial p}{\partial x}+\frac{\partial}{\partial x}(2\mu\frac{\partial u}{\partial x})+ \frac{\partial}{\partial y}[\mu(\frac{\partial u}{\partial y}+\frac{\partial v}{\partial x})]+\frac{\partial}{\partial z}[\mu(\frac{\partial u}{\partial z}+\frac{\partial w}{\partial x})] \qquad (2)$$

$$\frac{\partial \rho v^2}{\partial y}+\frac{\partial \rho uv}{\partial x}+\frac{\partial \rho vw}{\partial z}=-\frac{\partial p}{\partial y}+\frac{\partial}{\partial y}(2\mu\frac{\partial v}{\partial y})+ \frac{\partial}{\partial x}[\mu(\frac{\partial u}{\partial y}+\frac{\partial v}{\partial x})]+\frac{\partial}{\partial z}[\mu(\frac{\partial v}{\partial z}+\frac{\partial w}{\partial y})] \qquad (3)$$

$$\frac{\partial \rho w^2}{\partial z}+\frac{\partial \rho uw}{\partial x}+\frac{\partial \rho vw}{\partial y}=-\frac{\partial p}{\partial z}+\frac{\partial}{\partial z}(2\mu\frac{\partial w}{\partial z})+ \frac{\partial}{\partial x}[\mu(\frac{\partial w}{\partial x}+\frac{\partial u}{\partial z})]+\frac{\partial}{\partial y}[\mu(\frac{\partial w}{\partial y}+\frac{\partial v}{\partial z})] \qquad (4)$$

A Mac-type staggered grid system is used to locate the flow variables. The velocities are stored on the cell faces and the pressure is stored at the cell centres. Due to the staggering of the mesh three different types of control volume are required for the momentum equations and the continuity equation in the interior region, with straightforward modifications near the boundaries. A detailed description is given in [4].

The discrete equations are derived by first integrating the differential equations over each control volume surrounding the location of the variable. They are then expressed for a unit volume for convenient use of the multigrid technique. The fluxes over each control volume surface are constant. The resulting finite-difference set of algebraic equations (for grid dimensions dx, dy and dz) at each finite difference node (i, j, k) are as follows:

$$(A_c^u)_{i-1/2,j,k}\,u_{i-1/2,j,k}=F^u_{i-1/2,j,k} \qquad (5)$$

$$(A_c^u)_{i+1/2,j,k}\,u_{i+1/2,j,k}=F^u_{i+1/2,j,k} \qquad (6)$$

$$(A_c^v)_{i,j-1/2,k}\,v_{i,j-1/2,k}=F^v_{i,j-1/2,k} \qquad (7)$$

$$(A_c^v)_{i,j+1/2,k}\,u_{i,j+1/2,k}=F^u_{i,j+1/2,k} \qquad (8)$$

$$(A_c^w)_{i,j,k-1/2}\,w_{i,j,k-1/2}=F^w_{i,j,k-1/2,} \qquad (9)$$

$$(A_c^w)_{i,j,k+1/2}\,w_{i,j,k+1/2}=F^w_{i,j,k+1/2,} \qquad (10)$$

$$(u_{i+1/2,j,k}-u_{i-1/2,j,k})/\delta x+ (v_{i,j+1/2,k}-v_{i,j-1/2,k})/\delta y+ (w_{i,j,k+1/2}-w_{i,j,k-1/2})/\delta z=0, \qquad (11)$$

Where, for example:

$$F^u_{i+1/2,j,k} = A^u_n u_{i+1/2,j+1,i} + A^u_s u_{i+1/2,j-1,k}$$
$$+ A^u_e u_{i+3/2,j,k} + A^u_w u_{i-1/2,j,k} + A^w_l w_{i,j,k-1/2}$$
$$+ A^w_h w_{i,j,k+1/2} + (p_{i,j,k} - p_{i+1,j,k})/\rho\delta x +$$
$$\frac{\mu}{\rho\delta x\delta y}(v_{i+1,j+1/2,k} - v_{i,j+1/2,k} - v_{i+1,j-1/2,k}$$
$$+ v_{i,j-1/2,k}) + \frac{\mu}{\rho\delta x\delta z}(w_{i+1,j,k+1/2} - w_{i,j,k+1/2}$$
$$- w_{i+1,j,k-1/2} + w_{i,j,k-1/2}). \qquad (12)$$

The above equations can also be written in residual form as

$$R^u_{i-1/2,j,k} = F^u_{i-1/2,j,k} - (A^u_c)_{i-1/2,j,k} u_{i-1/2,j,k}, \quad (13)$$
$$R^u_{i+1/2,j,k} = F^u_{i+1/2,j,k} - (A^u_c)_{i+1/2,j,k} u_{i+1/2,j,k}, \quad (14)$$
$$R^v_{i,j-1/2,k} = F^v_{i,j-1/2,k} - (A^v_c)_{i,j-1/2,k} v_{i,j-1/2,k}, \quad (15)$$
$$R^v_{i,j+1/2,k} = F^v_{i,j+1/2,k} - (A^v_c)_{i,j+1/2,k} v_{i,j+1/2,k}, \quad (16)$$
$$R^w_{i,j,k-1/2} = F^w_{i,j,k-1/2} - (A^w_c)_{i,j,k-1/2} w_{i,j,k-1/2}, \quad (17)$$
$$R^w_{i,j,k+1/2} = F^w_{i,j,k+1/2} - (A^w_c)_{i,j,k+1/2} w_{i,j,k+1/2}, \quad (18)$$
$$R^c_{i,j,k} = F^c_{i,j,k} \qquad (19)$$

2. DERIVATION OF SCGS/LS IN 3D

The resulting finite-difference set of algebraic equations in terms of corrections and residuals along a paraxial line (say the y-axis), in the xy-plane at each finite difference node (i, j, k) are given below:

$$(A^u_c)_{i-1/2,j,k}\,\delta u_{i-1/2,j,k} + (\delta p_{i,j,k} - \delta p_{i-1,j,k})/\rho h = R^u_{i-1/2,j,k}, \quad (20)$$
$$(A^u_c)_{i+1/2,j,k}\,\delta u_{i+1/2,j,k} - (\delta p_{i,j,k} - \delta p_{i+1,j,k})/\rho h = R^u_{i+1/2,j,k}, \quad (21)$$
$$(A^v_c)_{i,j-1/2,k}\,\delta v_{i,j-1/2,k} + \delta p_{i,j,k}/\rho h = R^v_{i,j-1/2,k}, \quad (22)$$
$$(A^v_c)_{i,j+1/2,k}\,\delta v_{i,j+1/2,k} - \delta p_{i,j,k}/\rho h = R^v_{i,j+1/2,k}, \quad (23)$$
$$(A^w_c)_{i,j,k-1/2}\,\delta w_{i,j,k-1/2} + \delta p_{i,j,k}/\rho h = R^w_{i,j,k-1/2}, \quad (24)$$
$$(A^w_c)_{i,j,k+1/2}\,\delta w_{i,j,k+1/2} - \delta p_{i,j,k}/\rho h = R^w_{i,j,k+1/2}, \quad (25)$$
$$(\delta u_{i+1/2,j,k} - \delta u_{i-1/2,j,k})/h + (\delta v_{i,j+1/2,k} - \delta v_{i,j-1/2,k})/h$$
$$+ (\delta w_{i,j,k+1/2} - \delta w_{i,j,k-1/2})/h = R^c_{i,j,k}, \qquad (26)$$

Where δ's, are corrections, and h = δx = δy = δz is the uniform mesh size. Eliminate δu, δv and δw from (20-25) giving

$$\delta u_{i-1/2,j,k} = [R^u_{i-1/2,j,k} - (\delta p_{i,j,k} - \delta p_{i-1,j,k})/\rho h] / (A^u_c)_{i-1/2,j,k}, \qquad (27)$$
$$\delta u_{i+1/2,j,k} = [R^u_{i+1/2,j,k} + (\delta p_{i,j,k} - \delta p_{i+1,j,k})/\rho h] / (A^u_c)_{i+1/2,j,k}, \qquad (28)$$
$$\delta v_{i,j-1/2,k} = [R^v_{i,j-1/2,k} - \delta p_{i,j,k}/\rho h] / (A^v_c)_{i,j-1/2,k}, \qquad (29)$$
$$\delta v_{i,j+1/2,k} = [R^v_{i,j+1/2,k} + \delta p_{i,j,k}/\rho h] / (A^v_c)_{i,j+1/2,k}, \qquad (30)$$
$$\delta w_{i,j,k-1/2} = [R^w_{i,j,k-1/2} - \delta p_{i,j,k}/\rho h] / (A^w_c)_{i,j,k-1/2}, \qquad (31)$$
$$\delta w_{i,j,k+1/2} = [R^w_{i,j,k+1/2} + \delta p_{i,j,k}/\rho h] / (A^w_c)_{i,j,k+1/2} \qquad (32)$$

Substitute (27-32) back into (26) giving the required tri-diagonal system of equations in 3D to be solved,

$$(A^p_c)_{i+1,j,k}\,\delta p_{i+1,j,k} + (A^p_c)_{i,j,k}\,\delta p_{i,j,k} + (A^p_c)_{i-1,j,k}\,\delta p_{i-1,j,k} = R^p_{i,j,k}, \qquad (30)$$

$$(A^p_c)_{i+1,j,k} = -\frac{1}{\rho h^2 (A^u_c)_{i+1/2,j,k}},$$
$$(A^p_c)_{i-1,j,k} = -\frac{1}{\rho h^2 (A^u_c)_{i-1/2,j,k}},$$
$$(A^p_c)_{i,j,k} = [\frac{1}{(A^u_c)_{i+1/2,j,k}} + \frac{1}{(A^u_c)_{i-1/2,j,k}} + \frac{1}{(A^v_c)_{i,j+1/2,k}} + \frac{1}{(A^v_c)_{i,j-1/2,k}} + \frac{1}{(A^w_c)_{i,j,k+1/2}} + \frac{1}{(A^w_c)_{i,j,k-1/2}}]/\rho h^2,$$

Coefficients A^p_c and residuals $R^p_{i,j,k}$ are given as follows:

$$R^p_{i,j,k} = R^c_{i,j,k} - 1/h[R^u_{i+1/2,j,k}/(A^u_c)_{i+1/2,j,k} - R^u_{i-1/2,j,k}/(A^u_c)_{i-1/2,j,k}] - 1/h[R^v_{i,j+1/2,k}/(A^v_c)_{i,j+1/2,k} - R^v_{i,j-1/2,k}/(A^v_c)_{i,j-1/2,k}] - 1/h[R^w_{i,j,k+1/2}/(A^w_c)_{i,j,k+1/2} - R^w_{i,j,k-1/2}/(A^w_c)_{i,j,k-1/2}]$$

The 3D SCGS/LS algorithm solves equation (33) in a way similar to 2D ([2]) and gives the following new approximations

$$u^{new}_{i-1/2,j,k} = u^{old}_{i-1/2,j,k} + w_u \delta u_{i-1/2,j,k},$$
$$u^{new}_{i+1/2,j,k} = u^{old}_{i+1/2,j,k} + w_u \delta u_{i+1/2,j,k},$$
$$v^{new}_{i,j-1/2,k} = v^{old}_{i,j-1/2,k} + w_v \delta v_{i,j-1/2,k},$$
$$v^{new}_{i,j+1/2,k} = v^{old}_{i,j+1/2,k} + w_v \delta v_{i,j+1/2,k},$$
$$w^{new}_{i,j,k-1/2} = w^{old}_{i,j,k-1/2} + w_w \delta w_{i,j,k-1/2},$$
$$w^{new}_{i,j,k+1/2} = w^{old}_{i,j,k+1/2} + w_w \delta w_{i,j,k+1/2},$$
$$p^{new}_{i,j,k} = p^{old}_{i,j,k} + w_p \delta p_{i,j,k}.$$

3. MULTIGRID METHODS

There are several ways of multigrid cycling. We used FAS, suitable for non-linear problems. A detailed review of multigrid methods and variant strategies can be found in [6]. For grid coarsening we adopted a "continuity control volume lumping" ([4]), which ensures that the compatibility continuity condition between the fine and the coarse grid is satisfied. In short, each coarse grid continuity control volume is composed of four fine grid continuity control volumes. This follows the discrete compatibility condition on all grids, which is crucial to obtaining optimal multigrid convergence rates.

In the present study, the restricted coarse grid velocities are defined to be the mean of their two nearest neighbouring fine grid velocities. Coarse grid pressures are defined to be the mean of the four neighbouring fine grid pressures. The prolongation relations are derived by a bilinear interpolation. Details of restrictions and prolongations can be found in [4].

4. SMOOTHING PROCEDURE

In the present study, we developed a line solver for the coupled system of equations. We solved the derived Eqn. (33) for pressure corrections along a constant line, then a direct substitution into (27-32) yields values of the velocities along the same line. An under-relaxation parameter (ω_u, ω_v, ω_w) was implemented by dividing the coefficients A_c^u, A_c^v, A_c^w, respectively. The grid is scanned line by line in one direction followed by a similar sweep in the other direction taking the z-plane constant. The sweeps are repeated, in the multigrid strategy, until the desired convergence is obtained on the finest grid. The convergence criterion is based on the summed averaged residuals in the three equations.

5. LOCAL MODE ANALYSIS

To give an idea of the behavior of the relaxation schemes in iterative methods, local mode analysis is an efficient tool. Since the reduction of high frequency error components is essentially a local process, the analysis of this reduction need not take account of distant boundaries. Consider an arbitrary local section of the mesh with u, v, w velocities staggered along the x, y, z directions respectively and the pressure p located at nodes.

Assume that at the start of the smoothing process, errors in u, v, w and p are given (in Fourier modes) as follows:

$$\begin{bmatrix} \partial u \\ \partial v \\ \partial w \\ \partial p \end{bmatrix} = \begin{bmatrix} \partial u_0 \\ \partial v_0 \\ \partial w_0 \\ \partial p_0 \end{bmatrix} \exp(\iota\theta.X/h),$$

where $\theta.X/h = (\theta_{1x} + \theta_{2y} + \theta_{3z})/h$. Then, during the smoothing process, this singly corrected and the fully corrected errors are given by

$$\begin{bmatrix} \dot{\partial} u \\ \dot{\partial} v \\ \dot{\partial} w \end{bmatrix} = \begin{bmatrix} \partial u_1 \\ \partial v_1 \\ \partial w_1 \end{bmatrix} \exp(\iota\theta.X/h),$$

$$\begin{bmatrix} \ddot{\partial} u \\ \ddot{\partial} v \\ \ddot{\partial} w \\ \ddot{\partial} p \end{bmatrix} = \begin{bmatrix} \partial u_2 \\ \partial v_2 \\ \partial w_2 \\ \partial p_2 \end{bmatrix} \exp(\iota\theta.X/h),$$

and where ; ¨ denote singly and fully corrected values.

$$\begin{bmatrix} \partial u_2 \\ \partial v_2 \\ \partial w_2 \\ \partial p_2 \end{bmatrix} = M_{3d} \begin{bmatrix} \partial u_0 \\ \partial v_0 \\ \partial w_0 \\ \partial p_0 \end{bmatrix},$$

Notice that u, v and w are each corrected twice, but p only once. After some technical manipulation it can be shown that ([1]),

where M_{3d} is now the amplification matrix in 3D.

(δu_2, δv_2, δw_2, δp_2) and (δu_o, δv_o, δw_o, δp_o) are fully corrected and uncorrected values respectively. The smoothing factor in 3D is then given by

$$\bar{\mu} = \sup_{\theta \in h}[\rho(\mathrm{M}_{3d})],$$

where $\mathrm{H} = [-\pi, \pi]^3 \setminus [-\pi/2, \pi/2]^3$ is the set of high frequencies and $\theta = (\theta_1, \theta_2, \theta_3)$ are the Fourier components.

In the case of convection dominated flows, the above smoothing factor can be defined, in terms of frozen velocities u_0, v_0, w_0 are in order to maintain the relevant Reynolds number,

$$\bar{\mu} = \sup_{|u_0, v_0, w_0| \le \theta \in \mathrm{H}} [\rho(\mathrm{M}_{3d})].$$

6. SMOOTHING RATES

To obtain smoothing rates of the SCGS/LS, local mode analysis was carried out for the driven cavity problem in 3D. It is found that the underlying scheme has excellent smoothing capabilities especially at higher Reynolds numbers (Re > 1000). The SCGS/LS scheme is, indeed, far more efficient than other schemes like SIMPLE. This is because, for SCGS/LS, the practical smoothing rate remains well below the theoretical maximum at all Reynolds numbers. A comparison of SCGS and SIMPLE has been reported in [5]. A more detailed account of the theoretical smoothing capabilities of each of the schemes and plots of the reduction factors can be found in [1] and [3]. Here we give two plots of the amplification factors of the SCGS/LS scheme at Re = 100, and Re = 1000.

Fig. 1 shows the amplification factor at Re = 100 for flow direction (u_o, v_o, w_o) = (1, 0, 1). The smoothing factor in this case is equal to 0.56 compared with the 2D smoothing factor 0.57 ([2]). At such a low Reynolds number the amplification factor is independent of flow direction, which assures good smoothing capabilities for diffusion-dominated flows in 3D. Hence it validates the 2D assumptions that the 3D driven cavity can be well approximated in two dimensions.

Fig. 2 shows the amplification at Re = 1000 for flow direction (u_o, v_o, w_o) = (1, 0, 1). The smoothing rate in this case is also 0.56. This is the case of highly convective flows and the said scheme is proved efficient but at Re ≥ 5000 it gives a large smoothing factor. This is because the discrete ellipticity along such lines perpendicular to the flow direction is almost lost. A detail of such flows can be found in [1].

It is noticed that the worst part of the cavity is found at $\theta_3 = 0$, where the smoothing factor has become large. This is because at high Reynolds numbers (Re ≥ 5000) the strong secondary vortices appear at a plane $\theta_3 = 0$.

7. TEST PROBLEM

For the purpose of demonstrating the applicability and the robustness of the proposed scheme and to evaluate its performances relative to the earlier procedures [5], the driven cavity problem was solved. This test problem has been widely used for validating solution procedures for the Navier-Stokes equations. The underlying scheme is treated as a two-stage process. After solving a triple diagonal system of equations for pressures, velocities can be calculated by a direct substitution. The velocities are updated twice and the pressures once.

In order to get a grid independent convergence rate, the grid is swept line by line in alternating directions. This is achieved cheaply at low Reynolds numbers but it is more expensive, at higher Reynolds numbers, as we have to employ symmetric alternating directions. Numerical experiments show that symmetric alternating directions do not accelerate the convergence much at low Reynolds numbers (Re < 1000). The convergence criterion is based on the summed average residuals in the three equations i.e.,

$$R_{con} = sqrt\left(\frac{\sum_{i,j}[(R^u_{i,j})^2 + (R^v_{i,j})^2 + (R^w_{i,j})^2 + (R^c_{i,j})^2}{(4 \times i_{\max} \times j_{\max} \times k_{\max})}\right),$$

where R^u, R^v, R^w and R^c are residuals in the u, v, w momentum equations and in the continuity equation. i_{max}, j_{max}, k_{max} are the number of internal mesh points over which the summation is made. R_{con} was set to 10^{-4} and when the fine grid residual decreased below this value, the calculations were terminated. It is found to be the most efficient to carry out just one iteration in each cycle on every grid except the coarsest one. We solved the equations, on the coarsest grid, exactly by performing more than one local iteration.

8. RESULTS

The flow in a cubic cavity is an example of a real problem, was solved by using the underlying mltigrid method. Local mode analysis of this method was also carried out which predicted the rate of convergence of the multigrid method by smoothing factor. The convergence obtained by both local mode analysis and the numerical application of the multigrid method were very close agreement at low Reynolds numbers and slightly differed at high Reynolds numbers (Fig. 3). This is because the local mode analysis was performed on linear equations where as the actual application included all the nonlinearity of the Navier Stokes equations. Table (1) summarises the convergence characteristics of the multigrid method together with CPU time on VAX/785. It is seen that the relaxation parameters are quite high even for high Reynolds numbers, which was not the case in 2D. The cause of low relaxation parameter in 2D is mainly due to an approximation of three-dimensional problem in two-dimensional. Table (1) also indicates that the grid independent convergence rates are being approached at all Reynolds numbers.

Unlike 2D, three-dimensional solutions are difficult to present in graphical format, we could hardly produce the partical tracks in 3D, one can visualise the flow patterns in the lid-driven cavity. Figs. (4-5) are such pictures of the flow patterns and the velocity distribution at Re = 100 and Re = 1000 in side the

cavity. It is seen that at high Reynolds numbers the entire flow spread towards the wall of the cavity and generates high pressure at the centre of the cavity whereas at low Reynolds numbers the flow fills the entire cavity and the centre of the primary vortex to grow near the bottom front wall.

9. SUMMARY

The theoretical and practical smoothing capabilities of the proposed scheme (SCGS/LS) have been presented. The theoretical analysis showed that the underlying scheme has better h-independent convergence rates than SCGS at all Reynolds numbers, and in practice such convergence rates have been achieved. Numerical experiments demonstrated that such a solver is competitive in terms of execution time and simplicity of equations and coding, when compared to SIMPLE, SCGS and other schemes applied to complex incompressible flows. The scheme is robust in its insensitivity to the relaxation factors especially at the low Reynolds numbers.

Numerical experiments have shown that the underlying scheme converged monotonically even at Re = 20000. This showed the efficiency of the scheme; hence we further applied this method to solve problems like rectangular cavities with backward and forward steps.

10. REFERENCES

[1] T. M. Shah. Analysis of a multigrid method. Ph.D thesis, Oxford University, Oxford University Computing Laboratory, December 1989.

[2] T. M. Shah, D. F. Mayers, and J. S. Rollett. Analysis and Application of A Line Solver for the Recirculating Flows Using Multigrid Methods. In R. Rannacher W. Hackbusch, editor, Numerical Treatment of the Navier-Stokes Equations, pages 134-144, Braunschweig, January 1990. Vieweg.

[3] G. J. Shaw and S. Sivaloganathan. On the smoothing properties of the SIMPLE pressure correction algorithm. Inter. J. Num. Methods for Fluids, 8: 441-462, 1988.

[4] S. Sivaloganathan and G. J. Shaw. A multigrid method for Recirculating flows. Inter. J. Num. Methods for Fluids, 8: 417-440, 1988.

[5] S. Sivaloganathan, G. J. Shaw, T. M. Shaw, and D. F Mayers. Numerical Methods for Fluid Dynamics, page. Oxford University Press, March 1988.

[6] K. Stuben and U. Trottenberg. Multigrid Methods:, volume 960, pages 1-176. Lecture Notes in Mathematics, 1981

Table 1: Number of MG. iterations required to reduce residual norm 10^{-4}. (Figures in parentheses are CPU times on a VAX/VMS)

Finest Grid Re	2 6x6x6	3 18x10x10	4 18x18x18	5 34x34x34	6 66x66x66
100 ($\omega = 0.9$)	5 (.8s)	8 (8s)	8 (78s)	7 (740s)	8 (7386s)
400 ($\omega = 0.9$)	5 (.8s)	8 (11s)	7 (88s)	9 (945s)	9 (8339s)
1000 ($\omega = 0.9$)	7 (1.2s)	7 (7s)	8 (112s)	9 (945s)	10 (9256s)
5000* ($\omega = 0.7$)	16 (2.8s)	15 (16s)	14 (192s)	17 (1797s)	18 (19578s)
10000* ($\omega = 0.7$)	22 (3.9s)	25 (25s)	22 (315s)	25 (2643s)	26 (24036s)

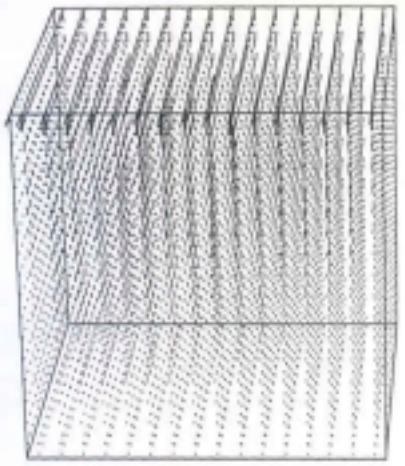

a)

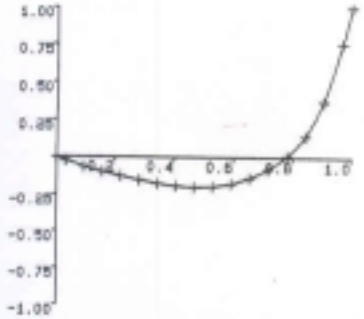

b)

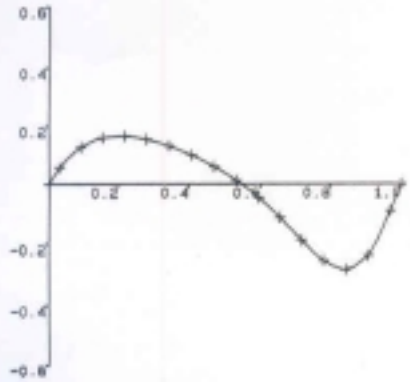

Fig. 4: a)Particle tracks for flow at Re=100; h=1/18
b)U on X=Y=0.5 at Re=100; h=1/18
c)W on Y=Z=0.5 at Re=100; h=1/18

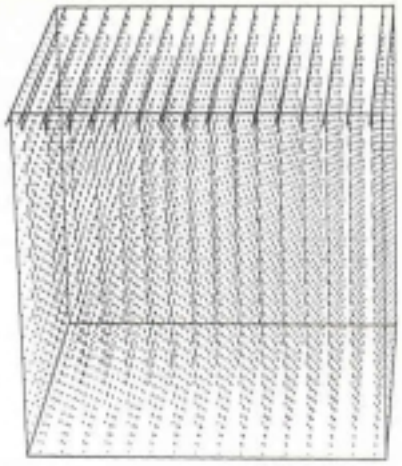

a)

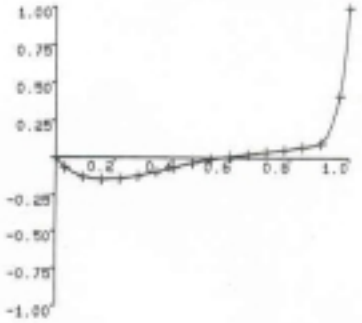

b)

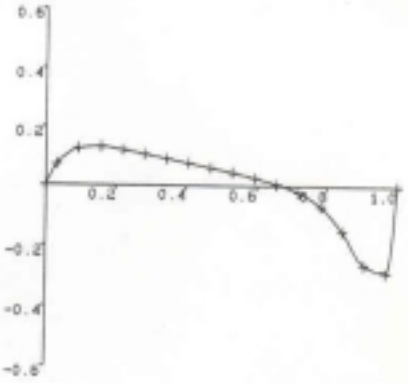

Fig. 5: a)Particle tracks for flow at Re=100; h=1/18
b)U on X=Y=0.5 at Re=100; h=1/18
c)W on Y=Z=0.5 at Re=100; h=1/18

Fig. 1: Amplification Factor at Reynolds Number 100 $(u_0, v_0, w_0) = (1, 0, 1); \theta_3 = 0$

Fig. 2: Amplification Factor at Reynolds Number 1000 $(u_0, v_0, w_0) = (1, 0, 1); \theta_3 = 0$

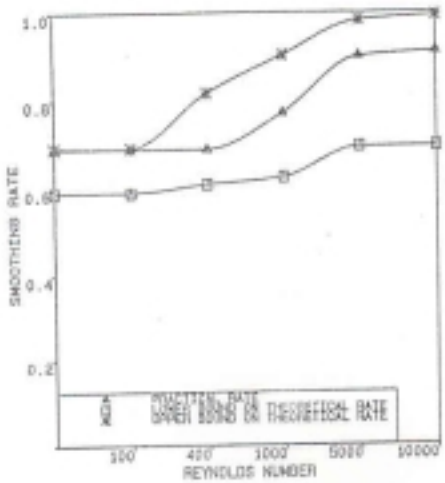

Fig. 3: Comparison of theoretical and practical smoothing rates